

Measurement of the *In Situ* Compressional Wave Properties of Marine Sediments

Gary B. N. Robb, Angus I. Best, Justin K. Dix, Paul R. White, *Member, IEEE*, Timothy G. Leighton, Jonathan M. Bull, and Andy Harris

Abstract—Geoacoustic inversion requires a generic knowledge of the frequency dependence of compressional wave properties in marine sediments, the nature of which is still under debate. The use of *in situ* probes to measure sediment acoustic properties introduces a number of experimental difficulties that must be overcome. To this end, a series of well-constrained *in situ* acoustic transmission experiments were undertaken on intertidal sediments using a purpose-built *in situ* device, the Sediment Probing Acoustic Detection Equipment (SPADE). Compressional wave speed and attenuation coefficient were measured from 16 to 100 kHz in medium to fine sands and coarse to medium silts. Spreading losses, which were adjusted for sediment type, were incorporated into the data processing, as were a thorough error analysis and an examination of the repeatability of both the acoustic wave emitted by the source and the coupling between probes and sediment. Over the experimental frequency range and source-to-receiver (S-R) separations of 0.99–8.1 m, resulting speeds are accurate to between $\pm 1.1\%$ and $\pm 4.5\%$ in sands and less than $\pm 1.9\%$ in silts, while attenuation coefficients are accurate to between ± 1 and ± 7 dB·m⁻¹ in both sands and silts. Preliminary results indicate no speed dispersion and an attenuation coefficient that is proportional to frequency.

Index Terms—Compressional wave attenuation, compressional wave speed, *in situ*, sediment.

I. INTRODUCTION

AN INCREASING number of marine applications, ranging from oil/gas prospecting [1], slope stability hazard assessment [2], and the siting of offshore structures [3] require knowledge of the geotechnical properties of seafloor sediments (e.g., porosity, density, and grain size). High-resolution subbottom reflection/refraction profiling permits the rapid, remote acquisition of the geoacoustic (i.e., compressional and shear wave) properties over large regions of the seafloor. Hence, there is significant interest in the inversion of these geoacoustic properties to obtain the geotechnical properties required for the aforementioned applications.

Manuscript received November 12, 2004; revised and accepted March 3, 2006. This work was supported in part by the Natural Environmental Research Council under Grant NER/S/A/2000/03621 and the Engineering and Physical Sciences Research Council under Grant EP/D000580/1.

Associate Editor: D. J. Tang.

G. B. N. Robb is with the National Oceanography Centre, Southampton, SO14 3ZH, U.K. and also with the Institute of Sound and Vibration Research, Southampton University, Southampton, SO17 1BJ, U.K. (e-mail: gbor199@noc.soton.ac.uk).

A. I. Best, J. K. Dix, J. M. Bull, and A. Harris are with the National Oceanography Centre, Southampton, SO14 3ZH, U.K.

P. R. White and T. G. Leighton are with the Institute of Sound and Vibration Research, Southampton University, Southampton, SO17 1BJ, U.K.

Digital Object Identifier 10.1109/JOE.2006.880430

Integral to such an approach is knowledge of the empirical and theoretical relationships between these geoacoustic properties and frequency. At present, the underlying physics behind the interaction of acoustic waves with sediment is still under debate. For example, a variety of relationships between the compressional wave attenuation coefficient and frequency have been proposed in the literature, including a linear relationship [4], various power-law relationships [5], and more complex relationships in which the frequency dependence relies on the frequency range under examination [6]. In addition, the question of whether compressional wave speed is dispersive or nondispersive is still contentious [7].

The use of *in situ* probes to measure compressional wave properties was pioneered in the 1950s [8]–[10]. Early work has been enhanced through the development and use of a number of *in situ* devices, e.g., acoustic lance [11], *in situ* sediment geoacoustic measurement system (ISSAMS) [12], and miniboomer [13]. Although there is a long history of good work in this field, the diversity of sediment types and the wide range of frequencies of interest, means that full coverage of the parameters necessary to test and refine theories requires further data. Furthermore, as the theoretical framework becomes increasingly developed, the ability to identify the uncertainties in input parameters and test data become increasingly valuable. One eventual goal of such a sustained effort might be to enable the frequency dependence of compressional wave properties being used as generic relationships which are applicable to all sediment types and frequencies.

The purpose of this paper is to present the development of an *in situ* acoustic measurement system developed to investigate the generic frequency dependence of both compressional wave speed and attenuation coefficient in marine sediment. Therefore, this paper will focus on the following:

- development of the Sediment Probing Acoustic Detection Equipment (SPADE) that allows frequencies from 16 to 100 kHz to be examined;
- use of the SPADE to perform *in situ* transmission experiments in a range of sediment types;
- presentation of processing techniques, which incorporate *in situ* spreading losses and a detailed analysis of intrinsic errors, to determine compressional wave speed and attenuation coefficient from transmission data.

Preliminary results have been presented to confirm the validity of the approach adopted, with an analysis of the complete data set to be discussed in future publications.

II. PREVIOUS *IN SITU* EXPERIMENTS

Three general acoustic techniques exist by which the compressional wave properties of marine sediments can be investi-

gated, namely the examination of sediment samples in the laboratory, remote reflection/refraction profiling, and *in situ* transmission experiments. Laboratory techniques allow external factors such as the pressure and temperature of the samples to be controlled [13], [14]. Potential drawbacks with this technique are that the collection, transportation, storage, and examination of the samples introduces an unknown degree of disturbance, while the limited sample size typically restricts the frequencies that can be examined to those greater than 200 kHz. Alternatively, remote techniques offer an efficient manner to measure the *in situ* acoustic properties of large volumes of surface and subsurface sediment [15]. Potential drawbacks with remote techniques are a degree of uncertainty in the volume of sediment insonified, while the processing techniques adopted require certain assumptions, which may restrict their use to certain sediment types [16].

In situ techniques offer a compromise between laboratory and remote techniques. Though *in situ* techniques are more invasive than remote techniques, they are less invasive than laboratory techniques. The experimental geometry associated with *in situ* transmission experiments is less constrained than for laboratory techniques and better characterized than for remote techniques. It provides a useful component to the balanced portfolio of techniques available for the acoustic characterization of marine sediment.

The earliest example of the use of *in situ* probes to measure the compressional wave properties of marine sediments was performed by Hamilton [8]–[10], who examined five discrete frequencies between 3.5 and 100 kHz. This work used source and receiver transducers attached to hollow stainless steel rods, which allowed sediment depths of 0.3–0.6 m and source-to-receiver (S-R) separations of 0.3–1 m to be investigated. Similarly, Wood and Weston examined five discrete frequencies from 4 to 48 kHz [17], using S-R separations from 0.4 to 60 m.

This early work has been advanced through the development of a number of *in situ* devices, which span a variety of frequency ranges. The deep-ocean sediment probe, which consists of four transducers located on the tips of the legs of a quad frame, was developed by Lewis [18]. This can penetrate 1.5 m into the seafloor and was used to examine the frequency range of 5–50 kHz in 5-kHz increments. McCann and McCann [19] used pipe transducers to examine intertidal sediments up to 2 m deep from 5 to 50 kHz, again in 5-kHz steps. Fu *et al.* investigate the lower frequency range of 5–20 kHz using the acoustic lance [11], which consists of ten receivers attached to a core barrel of length 3 m, with a source installed at the top of the corer. Turgut and Yamamoto [20] investigated 1–30 kHz, using four probes (a piezoceramic source and three receivers). These were deployed at depths of 4 m and S-R separations from 1 to 3 m using a hydraulic jet burial system. The range of lower frequencies used by subbottom profilers has been investigated using a miniboomer (1–11 kHz) [13], which utilizes S-R separations from 1 to 18 m. Conversely, frequencies more typical of high-resolution sonar have been examined using a profilometer, which can be attached to the cutter of a corer and operates at a nominal frequency of 200 kHz [21].

The most recent research in this field has utilized ISSAMS, which was initially developed by Richardson to operate at nom-

inal frequencies of 38 [22] and 58 kHz [23]. It uses four identical transducers on a fixed frame, with either one/two transducers acting as sources or two/three acting as receivers. The fixed frame allows S-R separation from 0.58 to 1 m and sediment depths up to 0.3 m to be examined. More recent work by Buckingham and Richardson [12] has extended the frequency range of ISSAMS to 25–100 kHz in frequency increments of 5 kHz. The same 5-kHz frequency step was used by Zimmer *et al.* [24], in extending the range from 15 to 200 kHz, although they expressed some concerns over the validity of the lower frequency data.

Bringing measurement techniques with laboratory accuracy to the seafloor presents many technical challenges, and is complicated by the natural variability in seafloor sediments (cf. laboratory samples that are generally chosen for their homogeneity). Overcoming these challenges allowed the previous research investigations to compile a body of data that has contributed to the development of the current array of models for acoustic propagation in marine sediments. As one goal is to determine the generic frequency dependence of compressional wave properties, it is useful for some individual studies to begin to examine both a broader variety of sediment types and a wider range of frequencies than was the norm for the pioneering studies mentioned previously. In an attempt to increase the certainty with which speed and attenuation results at different frequencies and seafloor locations can be compared, this paper sought to study the acoustic behavior of a wide range of sediment types over a wide range of frequencies, using a single device and methodology. The cost of this approach was that it was not possible to conduct experiments at wholly underwater sites, and instead the project concentrated on easily accessible intertidal sites (see Section V).

To generate data which allows generic frequency-dependent relationships to be examined, it is important to quantify the repeatability of the acoustic signal emitted by the source. The level of repeatability will depend on both the coupling of the transducers to the sediment, which has been qualitatively identified as a considerable source of variability in acoustic measurements [12], and the electronic signal transmitted to the source. Some processing techniques require that corrections for spreading losses are applied. While the assumption that spreading losses are the same in water and the sediment is approximately true in some cases, the use of *in situ* spreading losses would be more relevant. Finally, error analyses presented in the pioneering works cited previously generally refer to the standard deviation arising from variability. As the field matures, it is necessary to examine instead the intrinsic experimental error associated with the experimental and processing techniques adopted [12], [25]. This paper aims to build on previous research in this field to address in part some of the aforementioned issues.

III. SPADE, INCLUDING PULSE SELECTION

The SPADE comprises three acoustic components, namely a source and a pair of matched receivers, which are attached to 1.5-m-long aluminium channels (Fig. 1). The source consists of a section of piezoceramic material with a convex emitting face. This operates in an untuned manner over the usable frequency

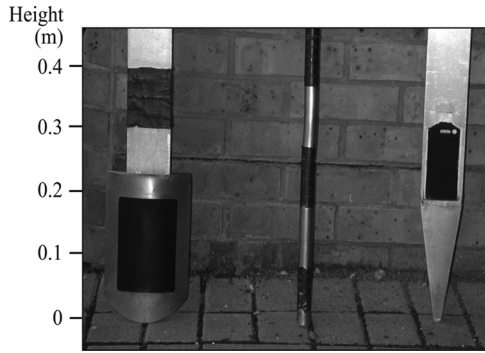


Fig. 1. SPADE source (left) and one of the receivers (right), both attached to aluminum channels to assist their deployment into the sediment.

range of 16–100 kHz. The transducer is embedded in a plastic mould, with a height of 158 mm, width of 109 mm, and thickness of 10 mm. A pair of matched receivers were used, each with a height of 119 mm, width of 58 mm, and thickness of 23 mm, the sensitivity of which varied from -189 to -198 dB re $1 \text{ V}/\mu\text{Pa}$ from 16 to 100 kHz. The acquisition system includes separate source and receiver amplifiers and a standard International Business Machines Corporation (IBM) compatible personal computer (PC). Trial transmission tests confirmed that the timing of the acquisition system was reliable to the sampling period of the acquisition card ($1 \mu\text{s}$), while amplitude was reliable to the resolution of the card (2.5 mV).

The waveforms utilized in the transmission experiments were tonal pulses, which were generated by passing a preprogrammed pulse through an amplifier and on to the source transducer. A suite of preprogrammed pulses was selected, each possessing ten cycles modulated by a Blackman–Harris envelope [27] with central frequencies f_i increasing from 16 to 100 kHz in comparatively fine increments of 2 kHz. The major factor limiting the experimental frequency range was the operational frequency range of the source amplifier. Pulses with central frequencies less than 16 kHz suffered considerable distortion (i.e., the ratio of the spectral amplitude of the second harmonic to the spectral amplitude of the fundamental frequency was greater than a defined threshold value of 0.15) while those greater than 100 kHz did not receive sufficient amplification. Typical examples of the voltage output pulse (VOP) transmitted from the source amplifier to the source transducer are displayed in Fig. 2(a)–(c). At central frequencies of 16–24 kHz, the frequency content of the pulses approached the lower limit of the operational bandwidth of the source amplifier. This resulted in nonlinear effects in the source amplifier, which generated harmonic components and produced tails on the voltage pulses at these frequencies. The effects of the source amplifier modified the central frequency of the VOP, f_o , to

$$f_o = 0.99f_i - 170 \text{ Hz.} \quad (1)$$

Signals received during calibration tests of the SPADE in water are displayed in Fig. 2(d)–(f). All signals are normalized to an amplitude of unity and, for comparison purposes, have the corresponding VOP overlain using time delays obtained from the cross correlation of the received signal and VOP

(Section VI). Hence, for propagation through water, the degree of distortion between the received and electronic pulses was negligible. Water calibration signals were found to be repeatable in time to $\pm 1 \mu\text{s}$ and in amplitude to $\pm 3.2\%$, values which account for the effects of the variability of the voltage signals on the emitted acoustic signal. This source of variability is incorporated into the error budget for the attenuation coefficients (Section VI-B).

Discrepancies between received signals detected during the field trials and the VOP were also minimal [see Fig. 2(g)–(i)]. This was a consequence of the use of pulses with smooth amplitude envelopes and the use of a frequency range over which the source transducer acted in an untuned manner and the receiving transducers possessed relatively flat sensitivities (quantified earlier in this section).

IV. PRESSURE FIELDS ASSOCIATED WITH THE SPADE

To allow the attenuation coefficient of the sediment to be measured, it was essential that the beam patterns associated with the SPADE are known. The receiver's beam pattern varies from an almost omnidirectional field at 1 kHz (which differs by less than 0.07 dB over a horizontal arc of 180° about the center of the receiver) to a much more directional field at 100 kHz (which displays 13 peaks and a variation of 0–77 dB over a similar arc). The relatively simple geometry of the transmission experiments (Section V) allowed estimated changes in the amplitude of the received signal, which arise from the receiver orientations, to be incorporated into the intrinsic error budget (Section VI-B).

The pressure field emitted by the source, which was required to apply corrections for *in situ* geometric spreading, was modeled using a modified version of a technique used to predict spreading losses for circular array transducers [28]. This allowed unique pressure fields to be predicted for each sediment type examined and, therefore, the application of *in situ* spreading losses in the processing techniques adopted (Section VI). This considered the source to be a segment of a cylinder from which sound radiates outwards (Fig. 3), i.e., an accurate representation of the SPADE source (Fig. 1). This segment was subdivided into a 2-D grid of elements, the dimensions of which were much less than the minimum wavelength of interest. Manipulation of (10) in [28] results in the following expression for the pressure at a field point X and angular frequency ω :

$$P(X, \omega) = W(\omega) dx dy \sum_{n=1}^{N_1} \sum_{m=1}^{N_2} \frac{e^{-i\omega R'/v} e^{-i\omega R_{n,m}/v}}{2\pi R_{n,m}} \quad (2)$$

where $W(\omega)$ is the spectrum of the selected voltage pulse, dx and dy are the size of the elements in the x and y directions, respectively, N_1 and N_2 are the number of integration steps in each direction, $R_{n,m}$ is the distance from source element n, m to field point X , and R' is the minimum distance between point X and the transducer surface. The pressure response at field point X associated with a given frequency ω can be obtained from the temporal maximum of the inverse fast Fourier transform (iFFT) of $P(X, \omega)$.

The parameters of r and θ in Fig. 3, which best define the SPADE source, were measured to be 146 mm (± 12 mm) and 42.9° ($\pm 0.03^\circ$), respectively. The surface elements used (length

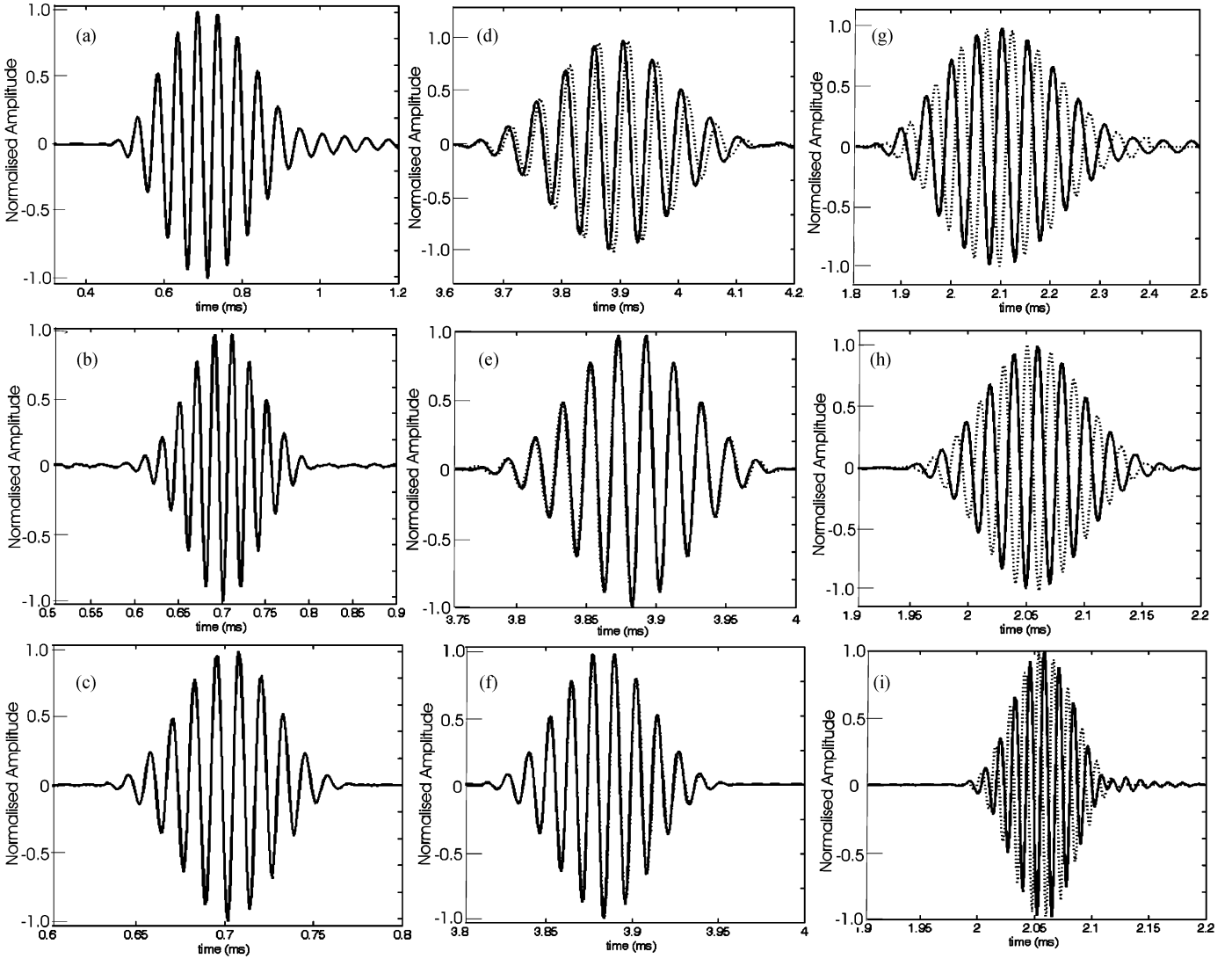


Fig. 2. Typical waveforms used, including the following: VOP with central frequencies of (a) 20 kHz, (b) 50 kHz, and (c) 80 kHz; calibration signals transmitted through water at (d) 20 kHz, (e) 50 kHz, and (f) 80 kHz; and signals transmitted through sediment at (g) 20 kHz, (h) 50 kHz, and (i) 80 kHz. To display the negligible differences between the calibration signals and sediment signals, a scaled, shifted version of the corresponding VOP (dashed lines) are displayed on (d)–(i). Note that all signals have been normalized to an amplitude of unity, while the varying time axes allow signals at different frequencies to be clearly displayed.

of 2 mm and an arc of 2 mm) satisfy the criterion that their dimensions are less than half the minimum wavelength examined (i.e., 13 mm) [28]. The use of 2048 samples in the iFFT prevents aliasing for the field points and frequencies of interest for the fieldwork performed. Finally, the pressure field was only computed for the horizontal plane that intercepts the center of the source, as the use of a common depth for source and receivers in the fieldwork performed (Section V) ensured that all receiver deployments lie in this plane. Deviations from this common depth are incorporated into the error budget (Section VI-B).

The model was verified through calibration signals measured using the SPADE source and receivers in a water tank. Transmitted signals were detected by placing the receivers in the horizontal plane that intercepts the center of the SPADE source. Measurements were taken along axes lying perpendicular to the face of the source and 5° clockwise and counterclockwise to this perpendicular. Receivers were placed at S-R separations from 3.49 to 6.49 m, at 0.5-m intervals. Five shots of each of the tonal pulses were recorded at all receiver locations.

The predicted decay in amplitude with S-R separation was compared to that observed for each angle and frequency. As the attenuation coefficient of water is less than $2.6 \times 10^{-3} \text{ dB}\cdot\text{m}^{-1}$ for frequencies less than 100 kHz [29], signal attenuation due to water was assumed to be negligible. Goodness of fit R^2 between the observed and modeled decay ranged from 0.79 and 1.00, representing a good to excellent fit. Discrepancies between the predicted and measured decays lay within the error limits in the experimental setup, i.e., $\pm 2^\circ$ in horizontal angle, $\pm 1^\circ$ in vertical angle, $\pm 0.02 \text{ m}$ in S-R separation, and $\pm 0.01 \text{ m}$ in depth. Hence, the pressure model described previously adequately predicts the pressure emitted by the SPADE source in nondispersive media.

Pressure fields were simulated for pulses with central frequencies from 16 to 100 kHz (in increments of 2 kHz) and compressional wave speeds from 1300 to 1800 $\text{m}\cdot\text{s}^{-1}$ (in increments of 100 $\text{m}\cdot\text{s}^{-1}$), i.e., the range of speed values obtained from field data analysis. Example pressure fields for pulses with central frequencies of 20, 50, and 80 kHz propagating through a medium with a compressional wave speed of 1600 $\text{m}\cdot\text{s}^{-1}$ are

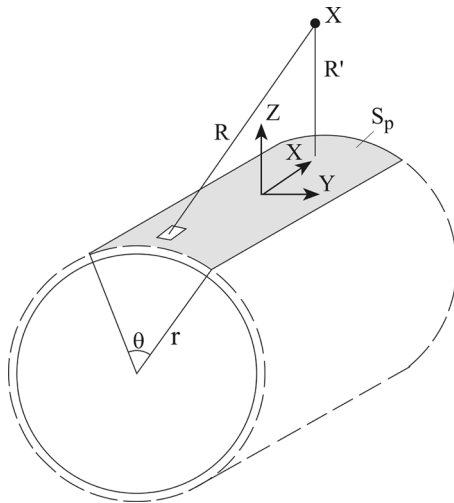


Fig. 3. Geometry used in the simulation of the pressure field emitted by the source, denoted by the shaded area segment S_p , modified from [28]. An example field point X is displayed, along with the distance R from source element dS , the minimum distance to the source R' , the parameters defining the source r and θ , and the coordinate system used.

displayed in Fig. 4. As the frequency increases, the pressure field becomes more directional, with sidelobes dominating over the central lobe at frequencies greater than 70 kHz. The unfocused nature of the pressure field is a consequence of the convex emitting face of the source. This angular dependence becomes more pronounced as the speed of the medium decreases.

The near-to-far-field transitions were computed as the distance from the center of the source along the axial line to the last maximum [30], [31]. This increases as the central frequency of the pulse increases and the compressional wave speed of the medium decreases. Near-to-far-field transitions lie less than 0.43 m from the source for all compressional wave speeds measured (1300–1800 $\text{m}\cdot\text{s}^{-1}$) and for all frequencies used (16–100 kHz).

One option for the processing is to assume certain properties of the beam pattern and spreading losses. Fig. 5 shows the difference in the pressure fields and beam patterns emitted at a frequency of 100 kHz in water ($v_w = 1470 \text{ m}\cdot\text{s}^{-1}$) and sand ($v_s = 1800 \text{ m}\cdot\text{s}^{-1}$). This scenario represents the most extreme difference, which reaches a maximum value of 2.6 dB at the sidelobes. This indicates that in this worst case example, if the spreading losses in sediment for SPADE have been assumed to be identical to those in water, errors of up to 25% could be possible in the received amplitudes. In fact, rather than assume a beam pattern based on either sound speed, the actual *in situ* pressure field data were used.

V. *IN SITU* EXPERIMENTS

A series of *in situ* experiments was performed using the SPADE on intertidal sediments along the south coast of England. While the use of intertidal sediments allows the source and receiver positions to be accurately measured, there is an increased risk of encountering partially saturated sediments. Partially saturated layers, which possess lower speeds than saturated sediments, have been observed in intertidal sediments [32]. To minimize the risk of encountering partially saturated

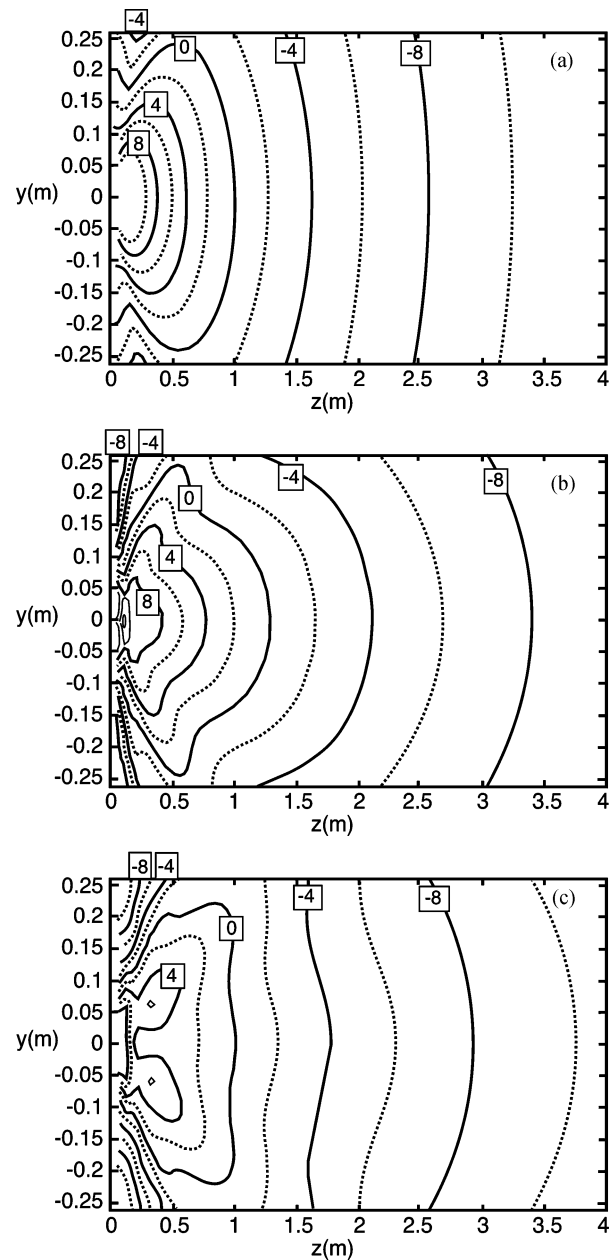


Fig. 4. Simulated pressure fields emitted by the SPADE source for a compressional wave speed of $1600 \text{ m}\cdot\text{s}^{-1}$ and central frequencies of (a) 20 kHz, (b) 50 kHz, and (c) 80 kHz. Solid contour lines are labeled in decibels, relative to the reference point, i.e., $z = 1$ and $y = 0$, while dashed lines indicate intermediate values, in increments of 2 dB.

sediments, sites examined were carefully selected to lie in coastal regions with low tidal ranges, with the tidal ranges at all sites examined less than 1.5 m.

It should be noted that, to date, published *in situ* acoustic measurements from “saturated” sediments assume full saturation. Gas bubbles can be introduced into marine sediment through a variety of mechanisms (e.g., the anaerobic decomposition of organic matter [33]) with numerous regions of gassy sediments observed across the world’s oceans [34]. As bubbles with diameters less than $500 \mu\text{m}$ cannot be resolved by the present measurement techniques available for gassy sediments (i.e., the x-ray computed tomography (CT) scanning of pressurized cores

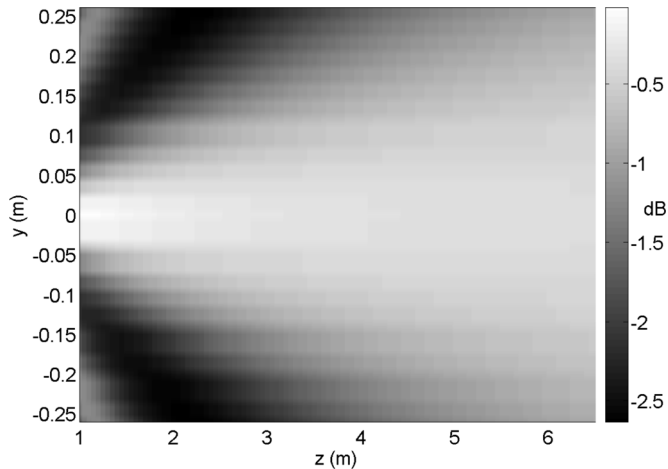


Fig. 5. Difference between simulated pressure fields at 100 kHz for compressional wave speeds of 1800 and 1470 $\text{m}\cdot\text{s}^{-1}$, plotted in decibels relative to the reference point.

[35]) such bubbles may be present in both intertidal and submerged sediments.

Six general sites were examined, including three sandy sites from Poole Harbour (sites 1–3), Dorset, and three silty sites from the Beaulieu estuary (site 4) and mouth of Southampton Water (sites 5 and 6), Hampshire, U.K. At each general site, between two and four specific locations were examined, to allow the variability of compressional wave properties across each site to be assessed.

The procedure involved inserting the source probe and a pair of receiver probes vertically into the sediment. The centers of the source and receivers were placed at a common depth of 1 m. This depth reduced the possibility of any interference from reflections from the seabed surface, while allowing sediment samples to be obtained from the sediment through which the acoustic waves propagated. The two receivers were deployed at approximately the same S-R separation astride the perpendicular to the source face (Fig. 6). While the experimental/processing techniques adopted herein only require a single source and receiver, the use of two receivers increased the quantity of data that could be collected. The receiver orientation adopted prevented the large receivers used from acoustically shadowing one another.

For the large transducers used in this paper, it is essential that the relative positions of the source and receivers were known. S-R separations, offsets, and depths were all measured to an accuracy of ± 0.01 m. The inclination of the probes was measured using a spirit level, and deviated from the vertical by less than $\pm 2^\circ$ for all deployments. Although the employment of a fixed frame would allow the relative positions and orientations of the probes to be more accurately measured, the use of individual channels (Fig. 1) allows increased flexibility in the S-R separations, and frequencies, which can be examined.

A series of acoustic pulses, consisting of five shots at each central frequency from 16 to 100 kHz, were then emitted by the source and detected by the receivers. The receivers were then removed and redeployed at a closer S-R separation and the same



Fig. 6. SPADE probe deployment during fieldwork, with receivers positioned at approximately the same S-R separation, lying on either side of the central line, which is marked by the measuring pole.

series of acoustic pulses acquired. Tidal windows permitted the examination of between three to seven S-R separations at each location.

In the silts, the source and receivers could be deployed through the manual application of a vertical force to the top of the aluminium channels. In the sands, this was not possible and, hence, a modified box corer (width 0.13 m and breadth 0.21 m) was used. This was initially inserted in the sediment to a depth of 1 m and the sand within it excavated. The probes were then inserted and, after the removal of the box corer, the sediment was refilled. This allowed the majority of sediment through which the acoustic pulses propagates to remain undisturbed, with the range of disturbed sediment around each probe (< 0.1 m) much less than the S-R separations examined (0.99–8.1 m). In addition, the S-R separations utilized ensured that all receivers were located in the far-field, while the successive use of closer S-R separations ensured that previous deployments did not disturb sediment that later deployments would reexamine.

At each location sediment samples were collected from a depth of 1 m and the temperature and salinity of the pore water were recorded. In addition, a push core with an inner diameter of 70 mm was collected from each site. The position and basic geotechnical properties of each site are displayed in Table I. Mean grain sizes were measured using 0.25ϕ sieve stacks for the predominantly sand samples and an optical particle size analyzer for the predominantly silt samples [7], with sediments classified using standard sedimentological procedures [36]. Porosity was obtained from gamma ray attenuation measurements on the cores, using a multisensor core logger [37] at a resolution of 1 cm. The basic geotechnical properties are presented in Table I, which quotes mean values with standard deviations.

TABLE I
GEOTECHNICAL PROPERTIES OF SITES

Site	Position	Sediment type	Mean grain size (ϕ)	No. samples	Porosity (%)
1	50° 40' 42-47'' N 001° 56' 56-58'' W	Mod well sorted Bimodal medium sand	1.58 ± 0.35	12	29.3 ± 1.0
2	50° 42' 23-29'' N 001° 54' 29'' W	Well sorted Unimodal medium sand	1.84 ± 0.15	6	32.9 ± 2.5
3	50° 41' 00-43'' N 001° 55' 54-55'' W	Well sorted Unimodal fine sand	2.16 ± 0.07	12	34.5 ± 1.7
4	50° 46' 39'' N 001° 23' 43-45'' W	Poorly sorted Unimodal medium silt	6.75 ± 0.30	9	80.1 ± 2.8
5	50° 52' 34-35'' N 001° 18' 43-44'' W	Poorly sorted Unimodal medium silt	6.77 ± 0.20	6	60.5 ± 2.1
6	50° 48' 56'' N 001° 18' 34'' W	V. poorly sorted Unimodal coarse silt	5.31 ± 0.15	6	63.2 ± 0.9

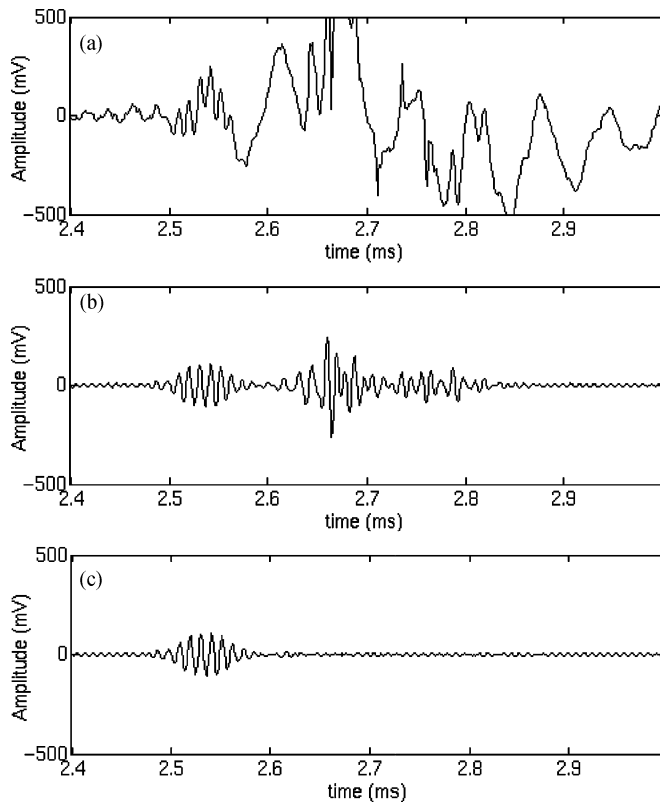


Fig. 7. Preprocessing steps applied to detected signals, including (a) typical received signal from the fieldwork, (b) output of the filtering stage, and (c) output of the stacking stage. The recovery of the directly transmitted signal from noisy raw data is clearly demonstrated.

VI. PROCESSING TECHNIQUES

The processing techniques outlined in this section include a thorough analysis of intrinsic errors, allow coupling repeatability to be broadly quantified, and do not assume any specific frequency dependence of attenuation coefficient or speed. Though these techniques do by necessity incorporate certain assumptions, the inclusion of a “coupling variability” in the error analysis accounts for deviations from these assumptions.

Commonly used preprocessing steps were applied to both the VOP and the received signals (Fig. 7). First, the signals were filtered using fifth-order Butterworth bandpass filters, the bandwidth of which varied with the central frequency of the pulse to ensure that a common fraction of “useful” energy was retained. Second, at each location, the five shots at each frequency and

S-R separation were stacked and the median of the stacked time series was found. The use of a median stack helped subdue the influence of random noise events, which under certain conditions dominate over the directly transmitted signal. The stacking stage improved the signal-to-noise ratio (SNR) by a factor of 1.78 [38].

A. Group Speed

A variety of techniques for determining speed were tested (see Appendix A), with the technique that was most stable for this data set presented here. This optimizes transmission data from a range of S-R separations, without requiring knowledge of the delay times incurred by the electronic components of the SPADE and acquisition system.

Analytical versions $\zeta(t)$ of both the VOP and received signals (which will be referred to as the analytical VOP and analytical received signals) were obtained from

$$\zeta(t) = y(t) + j\hat{y}(t) \quad (3)$$

where $y(t)$ is the preprocessed VOP or received signal and $\hat{y}(t)$ is the Hilbert transform of $y(t)$ [39], which is obtained from

$$\hat{y}(t) = y(t) * \frac{1}{\pi t} \quad (4)$$

where $*$ represents the convolution operator.

The analytical received signal was then correlated with the analytical VOP, and the time at which the correlation function peaks t_R was recorded. The arrival time t_A was then obtained from

$$t_A = t_R - t_o \quad (5)$$

where t_o is the time at which the cross-correlation function of the analytical VOP peaks.

The use of analytical signals means that the amplitude envelopes of the signals, rather than the actual signals, are correlated. For the data set examined, this approach was found to be more stable than phase-based techniques (see Appendix) and, hence, it was selected despite the increased errors introduced through the use of analytical signals.

The arrival time is the sum of the time taken for the acoustic pulse to propagate through the sediment and the time lag associated with both the source and receiver amplifiers and the moulding surrounding the transducers. Hence

$$t_A = \frac{d}{v_s} + t_L \quad (6)$$

where d is the S-R separation, v_s is the group speed of the sediment, and t_L is the cumulative time lag, which is fixed for all S-R separations at the same frequency. Hence, if arrival time is plotted against S-R separation for each frequency and a linear least-squares fit applied, the reciprocal of the gradient of the fit will represent the required group speed [Fig. 8(a)].

This approach assumes that the compressional wave speed of the sediment is constant over the volume of sediment examined and the amplitude envelopes of the VOP and received signals are the same for each location and frequency. The validity of the second assumption has been supported in Section III, with discrepancies between received signals and the VOP negligible for

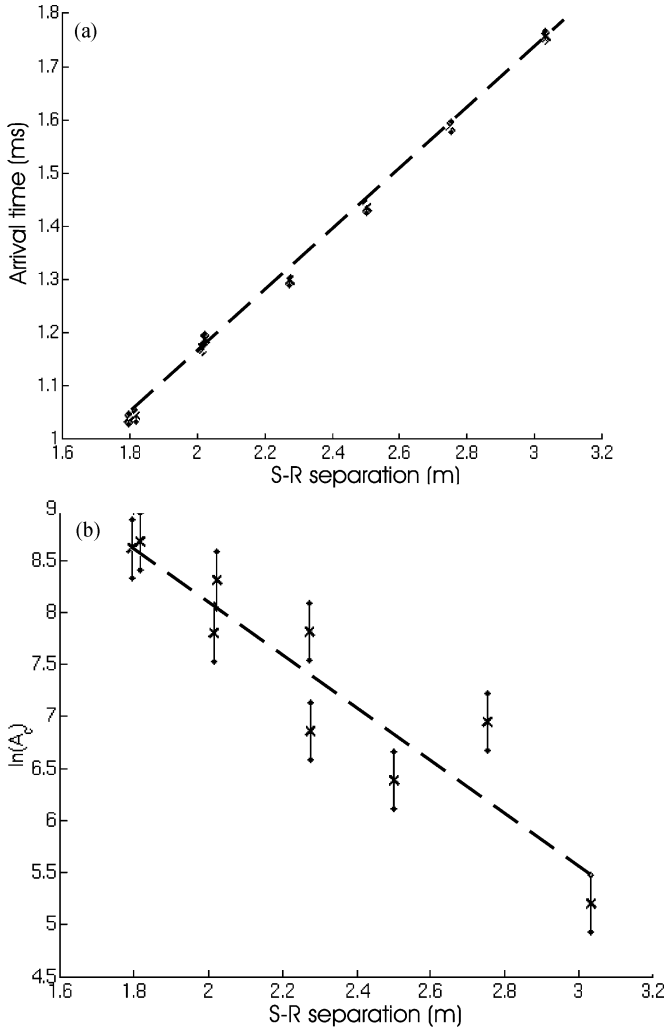


Fig. 8. Application of linear fits to transmission data at a single frequency (50 kHz), including (a) application of linear least-squares fit to arrival times versus S-R separation to obtain group speed and (b) application of weighted linear least-squares fit to natural logarithm of corrected amplitude versus S-R separation to obtain effective attenuation coefficient. Data points are plotted as crosses, with vertical bars denoting errors, while the linear least-squares fits are plotted as dashed lines.

the majority of signals detected during the field trials. In certain cases, the received signal was either undetectable above background noise, clipped, or disrupted by additional arrivals. Data arising from such distorted waveforms were manually identified and omitted from the analysis (see Appendix A).

The total error in arrival times t_E was calculated by combining the intrinsic timing error in the acquisition card ($\pm 1 \mu\text{s}$) with the error introduced into the correlation stage by the use of analytical signals ($\pm 10 \mu\text{s}$) in quadrature. This allowed the standard deviation in the speed σ_V , i.e., the relevant error, to be computed from

$$\sigma_V = \sqrt{\frac{t_E^2}{N(\bar{d}^2 - \bar{d}^2)}} \quad (7)$$

where N is the number of data points to which the linear fit is applied [40].

B. Attenuation Coefficient

The amplitude of the received pulse was recorded as the maximum peak-to-peak voltage of the received signal. To allow peak-to-peak voltages to produce reliable measures of amplitude, the received signal was interpolated to a sampling frequency of 10 MHz. For a given sediment, the resulting amplitude $A(f, d)$ is the outcome of the following processes:

$$A(f, d) = V_O(f)S_T(f)G(f, d)R_T(f)R_e(f)C e^{-\alpha_n(f)d} \quad (8)$$

where spreading losses $G(f, d)$ are a function of frequency and receiver location, the transmit voltage response (TVR) of the source transducer $S_T(f)$, the response of the receiving transducers $R_T(f)$, the electronic gain of the receiving transducers $R_E(f)$, and the attenuation of the sediment in $\text{Np}\cdot\text{m}^{-1}$ $\alpha_n(f)$ are all functions of frequency, and C represents the coupling parameter. Note that the attenuation and spreading losses will vary with the sediment under examination. The comparison of the received amplitudes at each frequency reduces the frequency-dependent terms to a constant B_1

$$A(d) = B_1 G(d) e^{-\alpha_n d}. \quad (9)$$

Spreading losses were accounted for using the pressure field simulated for the relevant frequency and compressional wave speed (Section IV). This was achieved by correcting the amplitude at a field point X by a factor of $10^{-dB(X)}$, where $dB(X)$ is the magnitude of the pressure field at field point X relative to a common reference point, which lies 1 m along the line perpendicular to the center of the source. Taking natural logarithms of the corrected amplitude A_C produces

$$\ln(A_C) = \text{const} - \alpha_n d. \quad (10)$$

Hence, at each location and frequency, $\ln(A_C)$ was plotted against d and a weighted linear least-squares fit applied, with the gradient of the fit equal to the effective attenuation coefficient in $\text{Np}\cdot\text{m}^{-1}$ [Fig. 8(b)]. The gradient approach assumes that the variability of the output pulse at each location and frequency is negligible (see Section VI-A) and the sediment volume examined at each location is homogeneous.

The variability of the coupling parameter C at each location and frequency was quantitatively examined using a “conditioned amplitude” A_{CO} . This was obtained by conditioning the measured amplitude to account for both geometric spreading (as aforementioned) and the attenuation of the sediment (through multiplication by a factor of $e^{-\alpha_n(d-1)}$) between the field point X and the common reference point. Hence, if signals from each location and frequency are considered individually, (8) can be reexpressed as

$$C = \frac{A_{CO}}{\text{const}}. \quad (11)$$

The mean percentage error associated with “coupling variability” at each location and frequency %CE can then be expressed as

$$\%CE = 100 \frac{\text{std}(A_{CO})}{\text{mean}(A_{CO})}. \quad (12)$$

The %CE varies from 0.3 to 60.6% for a random selection of locations examined, with a mean value of 27.4%. The lack of any observed relationship between %CE and either frequency or sediment justifies the incorporation of the mean coupling error into the following error analysis. The “coupling variability” term encompasses additional sources of error, such as sediment heterogeneity, the variability of the VOP, and uncertainty in the position and orientation of the probes, the last of which can introduce a maximum error of 7.6 dB into corrected amplitudes.

Errors in attenuation coefficient were computed by combining the following sources of error to obtain a total error in the corrected amplitude A_e .

- The resolution of the acquisition card with the increased SNR of the median stack incorporated (± 1.4 mV).
- The variability of the coupling parameter ($\pm 27.4\%$), which includes the error associated with coupling, sediment heterogeneity, variability of the VOP, and probe orientation/position.
- The prediction of spreading losses. For each location pressure fields were simulated for the measured compressional wave speed. The presence of intrinsic errors in speed introduces a degree of uncertainty into the predicted spreading losses. For all cases, this was less ± 0.1 dB and was included in the error budget.
- The uncertainty of the gain of the receiving amplifiers (± 0.224 dB).

As received amplitudes vary from 5.7 mV to 10 V, the second source of error represents the dominant component. The approximate error in each value of $\ln(A_C)$, which is termed Δ , was obtained from

$$\Delta = \frac{A_e}{A_C} \quad (13)$$

which produces a symmetric error, i.e., $\ln(A_C) \pm \Delta$. Hence, the error in the attenuation coefficient σ_α was obtained from

$$\sigma_\alpha = \sqrt{\frac{\overline{\overline{\Delta}}}{N \left(\overline{\overline{d^2}} - \overline{\overline{d}}^2 \right)}} \quad (14)$$

where a double overscore denotes a weighted mean [40].

The conversion of symmetric errors in A_C to a logarithmic scale will produce asymmetric errors in $\ln(A_C)$, i.e., $\ln(A_C) + \Delta_+$ and $\ln(A_C) - \Delta_-$, as opposed to the symmetric approximations used in the previous analysis; such an approach is required due to the absence of an alternative technique in the literature for fitting to asymmetric errors.

The effect of asymmetric errors on attenuation coefficients was estimated for one location at each of the six sites examined. The degree to which worst case scenarios differed from the previous analysis was assessed through the application of weighted least-square linear fits using the approximate errors ($\pm \Delta$), positive asymmetric errors ($\pm \Delta_+$), and negative asymmetric errors ($\pm \Delta_-$). The attenuation coefficient obtained from the three techniques differed by less than $0.07 \text{ dB}\cdot\text{m}^{-1}$, while σ_α obtained from the use of $\pm \Delta_+$ and $\pm \Delta_-$ differed from those obtained from the use of the approximate errors by less

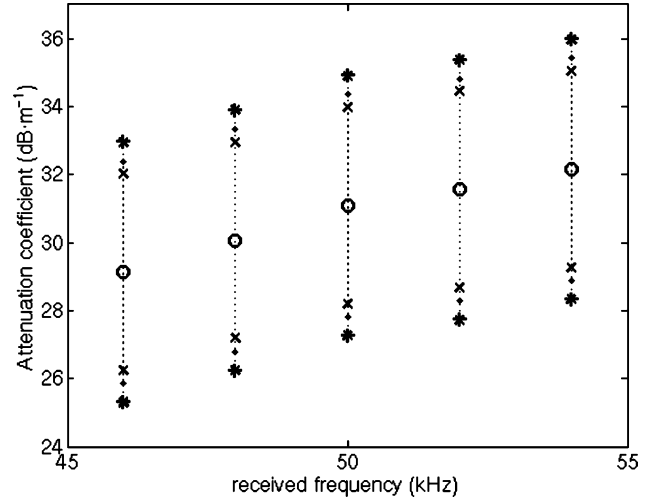


Fig. 9. Comparison of resulting attenuation coefficients arising from use of alternative errors in weighted least-squares linear fit for an example location and selected frequencies. Attenuation coefficients are denoted by circles, while errors are denoted by dots for approximate errors ($\pm \Delta$), crosses for positive asymmetric errors ($\pm \Delta_+$), and asterisks for negative asymmetric errors ($\pm \Delta_-$). Differences in attenuation coefficients are negligible, while errors in attenuation coefficient obtained from asymmetric errors differ from those obtained from the approximate errors by less than 17.5%.

than 17.5% (Fig. 9). Hence, the approach assumed previously is valid for the attenuation coefficients encountered and S-R separation utilized in this project. In different circumstances, e.g., greater attenuation coefficients or greater propagation distances, the previous approach may be invalid.

VII. PRELIMINARY RESULTS

Preliminary results for one location at each of the six intertidal sites examined are displayed in Fig. 10. Speed ratios vary from 1.06 to 1.26 in sands and 0.93 to 1.04 in silts, with intrinsic errors from $\pm 1.1\%$ to $\pm 4.5\%$ (± 20 to $\pm 70 \text{ m}\cdot\text{s}^{-1}$) in sands and less than $\pm 1.9\%$ ($< \pm 25 \text{ m}\cdot\text{s}^{-1}$) in silts. These speed ratios agree favorably with previously published measurements, e.g., speed ratios from 0.97 to 1.19 for a compilation of data spanning frequencies of 3.5–400 kHz and sediment porosities from 36% to 90% [41] and speed ratios from 0.93 to 0.99 which were measured on artificial clay/silt samples from 3 to 200 kHz [42].

Within the corresponding errors, speeds were found to be nondispersive in both sands and silts. Although, the compressional wave speed of marine sediments has been well examined, contention still exists over its frequency dependence. A significant volume of literature exists to support both dispersive relationships (e.g., [4], [13], and [43]) and nondispersive relationships (e.g., [12], [20], and [42]). This debate is reflected by existing geoaoustic models, with Grain–Shearing theory [44] predicting a weakly logarithmic dispersion at a rate of 1% per decade, while Biot theory predicts a more pronounced nonlinear relationship between speed and frequency [45], [46].

The effective attenuation coefficients of the intertidal sediments examined varied from 2 to $52 \text{ dB}\cdot\text{m}^{-1}$ in sands and 1 to $23 \text{ dB}\cdot\text{m}^{-1}$ in silts, with errors from ± 1 to $\pm 7 \text{ dB}\cdot\text{m}^{-1}$. These concur with previously published values that span a similar frequency range, e.g., *in situ* values of 8–60 $\text{dB}\cdot\text{m}^{-1}$, measured on

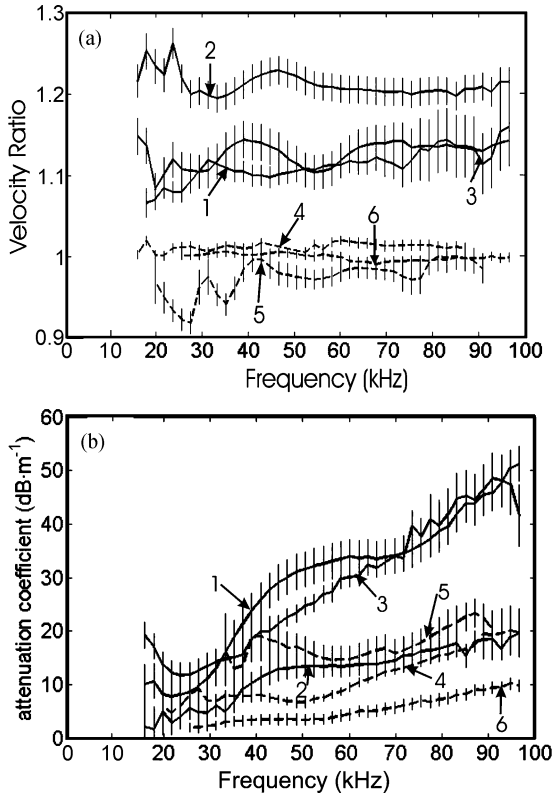


Fig. 10. (a) Example group speeds and (b) effective attenuation coefficients obtained from one location at each of the six sites examined, with sites labeled 1–6. Sands (sites 1–3) are denoted by solid lines, silts (sites 4–6) are denoted by the dashed lines, and errors are plotted as vertical bars.

sands from 25 to 100 kHz [12], and 0.6 to $74.3 \text{ dB}\cdot\text{m}^{-1}$, measured from 3.5 to 100 kHz in sediment types ranging from sands to clays [4]. For the majority of locations, examined attenuation coefficient is observed to be proportional to frequency from 16 to 100 kHz within the computed intrinsic errors.

As for speed, the frequency dependency of attenuation is currently under debate, with a suite of literature available to support attenuation coefficients which are both linearly (e.g., [4], [17], and [47]) and nonlinearly (e.g., [12], [13], and [42]) related to frequency. Again, the predictions of accepted geoaoustic models vary, with Biot theory [45], [46] predicting a nonlinear relationship between attenuation coefficient and frequency, while Grain–Shearing theory [44] predicting the almost linear relationship.

The results of a detailed examination of the compressional wave properties measured within this project will be presented in future publications. This will include a detailed statistical analysis of frequency dependency of speed and attenuation coefficient and a comparison between the measured properties and those predicted by certain geoaoustic models.

VIII. CONCLUSION

The main focus of this paper is to present the experimental and processing techniques adopted for a series of well-constrained *in situ* acoustic experiments. The restriction of this experiment to intertidal sediments permits a detailed investigation of the sources of uncertainty. The processing techniques

developed incorporate pressure fields applicable to the sediment under investigation, and an examination of the repeatability of the coupling between the transducers and the sediment. For the range of frequencies (16–100 kHz) and range of S-R separations examined (0.99–8.1 m) speeds are accurate to between $\pm 1.1\%$ and $\pm 4.5\%$ in sands and less than $\pm 1.9\%$ in silts, while attenuation coefficient is accurate to between ± 1 and $\pm 7 \text{ dB}\cdot\text{m}^{-1}$ in both sands and silts (note that errors relate to the intrinsic experimental errors, rather than reflecting the use of standard deviations arising from variability). Preliminary results indicate that within errors, speed is nondispersive and attenuation coefficient is proportional to frequency. Future papers will present a detailed investigation of the frequency dependence of compressional wave properties and a comparison between measured properties and those predicted by geoaoustic models.

APPENDIX COMPARISON OF PROCESSING TECHNIQUES FOR DETERMINING SPEED

A variety of processing techniques for determining speed were tested for the *in situ* data set collected. Each technique can be divided into two stages, namely the measurement of arrival times from the preprocessed signals and the conversion of these arrival times into group speeds. The first stage can be achieved through either the time-based correlation of analytical signal (outlined in Section VI-A) or an alternative phase-based approach.

For each central frequency and S-R separation, this phase-based approach entailed calculating the cross spectrum S_{xy} of the preprocessed received signal and corresponding VOP

$$S_{xy} = X(f)\tilde{Y}(f) = |S_{xy}(f)| e^{j\varphi_{xy}(f)} \quad (\text{A1})$$

where $X(f)$ and $Y(f)$ are the normalized spectra of the VOP and the received signals, respectively, and $\varphi_{xy}(f)$ is the phase of the cross spectrum. Both signals were windowed to include the entirety of the pulses of interest and omit undesirable noise events. If the effect of the sediment is purely to delay the pulse (i.e., the received waveform is simply a shifted and scaled version of VOP) the group delay time τ can be determined from the gradient of unwrapped phase versus frequency. To include frequencies at a sufficient SNR, this slope was determined for the frequency band spanning $f_c \pm 0.5 \cdot B_w$, where f_c represents the central frequency of the pulse and B_w represents the corresponding bandwidth. The quality of a linear fit to the unwrapped phases and so the validity of the previous assumption were quantified through E_P , which is defined by

$$E_P = \frac{Y(f)}{X(f)e^{-2\pi j f \tau}} = |E_P| e^{j\varphi_E} \quad (\text{A2})$$

where φ_E is the unwrapped phase of E_P . For a pure delay, φ_E should be constant, hence, the range of φ_E over the frequency band under consideration is employed as a quantitative measure of the quality of the linear fit.

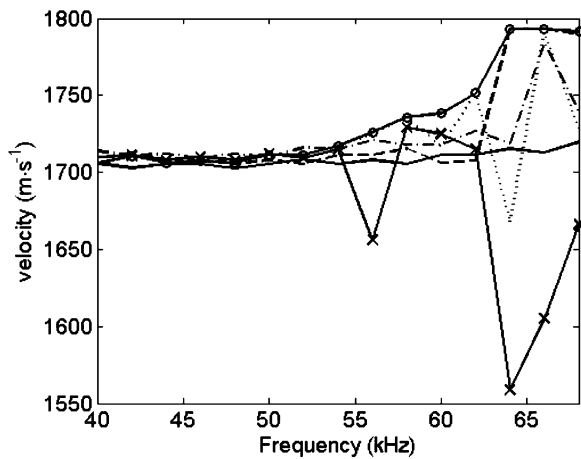


Fig. 11. Group speeds obtained from an example sand location for the frequency range of 40–70 kHz. Group speeds obtained using six processing techniques adopted are displayed, including CM technique (solid line), CE technique (dashed line), CR technique (dash-dot line), PM technique (dotted line), PE technique (circles), and PR technique (crosses).

The second stage determined the speed at each central frequency through the application of a linear fit of arrival times to S-R separation (see Section VI-A). This approach was required to account for the unknown delay time introduced by the SPADE. Both of the techniques under consideration for obtaining arrival times assume that the received pulse is a shifted version of VOP pulse, which in certain cases was not applicable. It was, therefore, necessary to identify and account for data points arising from distorted waveforms. This could be achieved using three methods, the first of which involved manual observation of distorted waveforms and omission of corresponding arrival times. The second method omitted data corresponding to a range of φ_E greater than a certain threshold value, while the third used a robust bisquares fit [48] to account for outliers.

The combination of the variety of techniques for the two stages resulted in six manners in which group speed could be computed, which include the following:

- use of a temporal correlation with manual identification of distorted waveforms (termed CM technique);
- use of a temporal correlation with distorted waveforms identified using the range of φ_E (termed CE technique);
- use of a temporal correlation with distorted waveforms accounted for using robust least-squares (termed CR technique);
- use of the phase of the cross spectra with manual identification of distorted waveforms (termed PM technique);
- use of the phase of the cross spectra with distorted waveforms identified using the range of φ_E (termed PE technique);
- use of the phase of the cross spectra with distorted waveforms accounted for using robust least-squares (termed PR technique).

Example results are displayed for sand and silt locations in Figs. 11 and 12, respectively. The selection criterion used to determine the best technique assumed that the difference between speeds determined at adjacent central frequencies, which differ by 2 kHz, should be minimal. This is justified by the examination of saturated sediments under examination, the use of a

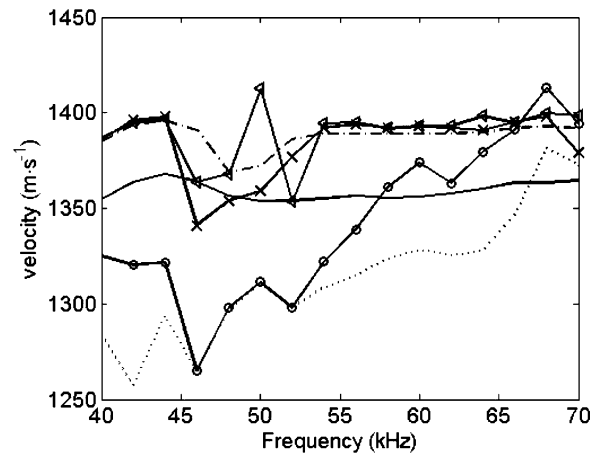


Fig. 12. Group speeds obtained from an example silt location for the frequency range of 40–70 kHz. Group speeds obtained using the six processing techniques adopted are displayed, including CM technique (solid line), CE technique (triangles), CR technique (dash-dot line), PM technique (dotted line), PE technique (circles), and PR technique (crosses).

common pulse envelope for all tonal pulses, and the untuned nature of the source and receivers (see Section III). For all trial data sets examined, the CM technique resulted in the least difference between speeds at adjacent frequencies, with other techniques proving less stable for this *in situ* data set.

A disadvantage of the correlation-based technique selected is the increased error introduced into speed through the use of analytical signals (see Section VI-A), as opposed to phase-based techniques which use the carrier wave and so limit temporal errors to $\pm 1 \mu\text{s}$. However, the increased stability of the CM technique supports its use for obtaining group speeds for this data set (see Section VI-A).

ACKNOWLEDGMENT

The authors would like to thank The National Trust, English Nature, Poole Borough Council, Poole Harbour Commission, The Beaulieu Estate, G. Korab, and the management of Mercury and Universal Marinas (Hamble River, Hampshire, U.K.), for granting permission to survey the intertidal sites. They would also like to thank R. Apprioual, S. Arnott, P. Cole, C. Cooil, J. Davies, S. Dean, M. Gutowski, and R. Saunders for fieldwork assistance.

REFERENCES

- [1] R. E. Sheriff and L. P. Geldart, *Exploration Seismology*. Cambridge, U.K.: Cambridge Univ. Press, 1995, ch. 14.
- [2] J. Locat and J. Mienert, *Submarine Mass Movements and their Consequences*. Dordrecht, The Netherlands: Kluwer, 2003.
- [3] J. J. Myers, *Handbook of Ocean and Underwater Engineering*. New York: McGraw-Hill, 1969, ch. 8.
- [4] E. L. Hamilton, "Compressional-wave attenuation in marine sediments," *Geophys.*, vol. 37, no. 4, pp. 620–646, 1972.
- [5] A. C. Kibblewhite, "Attenuation of sound in marine sediments: A review with emphasis on new low frequency data," *J. Acoust. Soc. Amer.*, vol. 86, no. 2, pp. 716–738, 1989.
- [6] R. D. Stoll, *Sediment Acoustics*. Berlin, Germany: Springer-Verlag, 1974, ch. 1.
- [7] G. B. N. Robb, "The *in situ* compressional wave properties of marine sediments," Ph.D. dissertation, Inst. Sound Vibration Res., Univ. Southampton, Southampton, U.K., 2004.
- [8] E. L. Hamilton, G. Shumway, H. W. Menard, and C. J. Shipke, "Acoustic and other properties of shallow-water sediments off San Diego," *J. Acoust. Soc. Amer.*, vol. 28, pp. 1–15, 1956.

- [9] E. L. Hamilton, "Sediment sound velocity measurements made in situ from bathyscaph Trieste," *J. Geophys. Res.*, vol. 68, no. 21, pp. 5991–5998, 1963.
- [10] E. L. Hamilton, "Sound velocity and related properties of marine sediments, North Pacific," *J. Geophys. Res.*, vol. 75, no. 23, pp. 4423–4446, 1970.
- [11] S. S. Fu, R. H. Wilkens, and L. N. Frazer, "Acoustic Lance: New in situ seafloor velocity profiles," *J. Acoust. Soc. Amer.*, vol. 99, no. 1, pp. 234–242, 1996.
- [12] M. J. Buckingham and M. D. Richardson, "On tone-burst measurements of sound speed and attenuation in sandy marine sediments," *IEEE J. Ocean. Eng.*, vol. 27, no. 3, pp. 429–453, Jul. 2002.
- [13] A. I. Best, Q. J. Huggett, and A. J. K. Harris, "Comparison of in situ and laboratory acoustic measurements on Lough Hyne marine sediments," *J. Acoust. Soc. Amer.*, vol. 110, no. 2, pp. 695–709, 2001.
- [14] M. D. Richardson and K. B. Briggs, "On the use of acoustic impedance values to determine sediment properties," *Proc. Inst. Acoust.*, vol. 15, no. 2, pp. 15–23, 1993.
- [15] I. R. Stevenson, C. McCann, and P. B. Runciman, "An attenuation-based sediment classification technique using Chirp sub-bottom profiler data and laboratory analysis," *Mar. Geophys. Res.*, vol. 23, pp. 277–298, 2002.
- [16] G. B. N. Robb, P. R. White, J. M. Bull, A. I. Best, T. G. Leighton, and J. K. Dix, "The estimation of geoacoustic properties from broadband acoustic data, focusing on instantaneous frequency techniques" Inst. Sound Vibration Res., Southampton, U.K., Tech. Rep. 298, 2002.
- [17] A. B. Wood and D. E. Weston, "The propagation of sound in mud," *Acustica*, vol. 14, pp. 156–162, 1964.
- [18] L. F. Lewis, "An investigation of ocean sediments using the deep ocean sediment probe," Ph.D. dissertation, Dept. Ocean Eng., Univ. Rhode Island, Kingston, RI, 1971.
- [19] C. McCann and D. M. McCann, "A theory of compressional wave attenuation in noncohesive sediments," *Geophys.*, vol. 50, no. 8, pp. 1311–1317, 1985.
- [20] A. Turgut and T. Yamamoto, "Measurements of acoustic wave velocities and attenuation in marine sediments," *J. Acoust. Soc. Amer.*, vol. 87, no. 6, pp. 2376–2383, 1990.
- [21] D. J. Shirley and A. L. Anderson, "In situ measurement of marine sediment acoustical properties during coring in deep water," *IEEE Trans. Geosci. Electron.*, vol. GE-13, no. 4, pp. 163–169, 1975.
- [22] M. D. Richardson, D. L. Lavoie, and K. B. Briggs, "Geoacoustic and physical properties of carbonate sediments of the Lower Florida keys," *Geo-Mar. Lett.*, vol. 17, pp. 316–324, 1997.
- [23] M. D. Richardson and K. B. Briggs, "In situ and laboratory geoacoustic measurements in soft mud and hard-packed sand sediments: Implications for high-frequency acoustic propagation and scattering," *Geo-Mar. Lett.*, vol. 16, pp. 196–203, 1996.
- [24] M. A. Zimmer, L. D. Bibee, and M. D. Richardson, "Acoustic sound speed and attenuation measurements in seafloor sands at frequencies from 1 to 400 kHz," in *Proc. Int. Conf. Underwater Acoust. Meas.: Technol. Results*, Heraklion, Crete, Greece, Jun. 28–Jul. 1 2005, pp. 327–334.
- [25] K. L. Williams, D. P. Jackson, E. I. Thoros, D. Tang, and S. Schock, "Comparison of the sound speed and attenuation measured in a sandy sediment to predictions based on the Biot theory of porous media," *IEEE J. Ocean. Eng.*, vol. 27, no. 3, pp. 413–428, Jul. 2002.
- [26] D. J. Janssen, J. Voss, and F. Theilen, "Comparison of methods to determine Q in shallow marine sediments from vertical reflection seismograms," *Geophys. Prospecting*, vol. 33, pp. 479–497, 1985.
- [27] S. G. Schock, L. R. LeBlanc, and L. A. Mayer, "Chirp sub-bottom profiler for quantitative sediment analysis," *Geophys.*, vol. 54, no. 4, pp. 445–450, 1989.
- [28] J. M. G. Borsboom, E. I. Cespedes, A. F. W. Van der Steer, C. T. Lancee, and E. F. Deprettere, "Simulation of circular array ultrasound transducers for intravascular applications," *J. Acoust. Soc. Amer.*, vol. 108, no. 2, pp. 827–835, 2000.
- [29] M. Schulkin and H. W. Marsh, "Absorption of sound in seawater," in *Proc. Symp. Sonar Syst.*, 1962, pp. 1–23.
- [30] L. E. Kinsler, A. R. Frey, A. B. Coppens, and J. V. Sanders, *Fundamentals in Acoustics*. New York: Wiley, 1982, ch. 8.
- [31] T. G. Leighton, *The Acoustic Bubble*. London, U.K.: Academic, 1994, ch. 1.
- [32] R. Bachrach and A. Nur, "High-resolution shallow-seismic experiments in sand, Part I: Water table, fluid flow and saturation," *Geophys.*, vol. 63, no. 4, pp. 1225–1233, 1998.
- [33] D. D. Rice and G. E. Claypool, "Generation, accumulation and resource potential of biogenic gas," *Amer. Assoc. Petroleum Geologists Bull.*, vol. 65, pp. 5–25, 1981.
- [34] P. Fleischer, T. H. Orsi, M. D. Richardson, and A. L. Anderson, "Distribution of free gas in marine sediments: A global overview," *Geo-Mar. Lett.*, vol. 21, pp. 103–122, 2001.
- [35] A. I. Best, M. D. J. Tuffin, J. K. Dix, and J. M. Bull, "Tidal height and frequency dependence of acoustic velocity and attenuation in shallow gassy marine sediments," *J. Geophys. Res.*, vol. 109, no. B8, 2004, DOI: 10.1029/2003JB002748, Art. no. B08101.
- [36] J. McManus, M. Tucker, Ed., "Grain size determination and interpretation," in *Techniques in Sedimentology*. London, U.K.: Blackwell Science, 1989, pp. 63–85.
- [37] A. I. Best and D. G. Gunn, "Calibration of multi-sensor core logger measurements for marine sediment acoustic impedance studies," *Mar. Geology*, vol. 160, no. 1–2, pp. 137–146.
- [38] H. Cramer, *Mathematical Methods of Statistics*. Princeton, NJ: Princeton Univ. Press, 1946, ch. 28.
- [39] L. Cohen, *Time-Frequency Analysis*. Englewood Cliffs, NJ: Prentice-Hall, 1995, ch. 2.
- [40] R. J. Barlow, *Statistics: A Guide to the Use of Statistical Methods in the Physical Sciences*. Chichester, U.K.: Wiley, 1989, ch. 6.
- [41] M. J. Buckingham, "Compressional and shear wave properties of marine sediments: Comparisons between theory and data," *J. Acoust. Soc. Amer.*, vol. 11, no. 1, pp. 137–152, 2005.
- [42] L. D. Hampton, "Acoustical properties of sediments," *J. Acoust. Soc. Amer.*, vol. 42, pp. 882–890, 1967.
- [43] E. G. McLeroy and A. Deloach, "Sound speed and attenuation, from 15 to 1500 kHz, measured in natural seafloor sediments," *J. Acoust. Soc. Amer. (Letters to the Editor)*, pp. 1148–1150, 1968.
- [44] M. J. Buckingham, "Compressional and shear wave properties of marine sediments: Comparisons between theory and data," *J. Acoust. Soc. Amer.*, vol. 117, pp. 137–152, 2005.
- [45] M. A. Biot, "Theory of propagation of elastic waves in fluid-saturated porous solids: 1. Low-frequency range," *Journal of the Acoustical Society of America*, vol. 28, pp. 168–178, 1956.
- [46] M. A. Biot, "Theory of propagation of elastic waves in fluid-saturated porous solids: 2. Higher frequency range," *J. Acoust. Soc. Amer.*, vol. 28, pp. 179–191, 1956.
- [47] E. L. Hamilton, A. Lara-Saenz, C. Ranz-Guerra, and C. Carbo-Fite, Eds., "Acoustic properties of sediments," in *Acoustics and the Ocean Bottom*. Madrid, Spain: CSIC, 1987, pp. 3–58.
- [48] W. H. Press, B. P. Flannery, S. A. Teukolsky, and W. T. Vetterling, *Numerical Recipes: The Art of Scientific Computing*. Cambridge, U.K.: Cambridge Univ. Press, 1987, ch. 2.



Gary B. N. Robb received the M.S. degree in physics from Oxford University, Oxford, U.K., in 1997, the M.S. degree in oceanography from the University of Southampton, Southampton, U.K., in 2000, and the Ph.D. degree in sediment acoustics from the University of Southampton, Southampton, U.K., in 2004, which focused on the *in situ* acoustic properties of saturated sediments.

Currently, he is a Research Fellow at the National Oceanography Centre Southampton, University of Southampton. His present research focuses on the

investigation of the acoustic properties of gassy sediments, incorporating both theoretical elements and *in situ* measurements.



Angus I. Best received the B.Sc. degree in geological geophysics, in 1988 and the Ph.D. degree in geophysics, in 1993, both from the University of Reading, Reading, U.K.

He was a Postdoctoral Researcher at the University of Reading for two years. In 1995, he joined National Oceanography Centre, Southampton, University of Southampton, Southampton, U.K., as a Research Geophysicist. His current research interests include the acoustic properties marine sediments, gassy sediments and gas hydrate-bearing sediments,

and the seismic properties of petroleum reservoir rocks. Applications include seafloor geotechnical surveying, geohazard prediction (e.g., slope stability), and reservoir characterization (hydrocarbons, water, CO₂ storage).



Justin K. Dix received the B.Sc. degree in geology from the University of Dundee, Dundee, Scotland, U.K., and the Ph.D. degree in marine geophysics from University of St Andrews, Fife, Scotland, U.K.

He holds the first ever post created in marine geophysics and archaeology in the United Kingdom, and the first cross Science-Arts Faculty position at the University of Southampton, Southampton, U.K. His current research interests include the development of new high-resolution acoustic tools for marine investigation, geoacoustic and geotechnical characteristics

of marine sediments with particular emphasis on shallow gas deposits, and identification, reconstruction, and *in situ* preservation of submerged archaeological sites.



Paul R. White (M'00) received the Ph.D. degree from Institute of Sound and Vibration Research, University of Southampton, Southampton, U.K., in 1992

Currently, he is a Professor of Statistical Signal Processing at University of Southampton. His research interests are in digital signal processing (DSP), in particular, application of DSP to problems in underwater acoustics, condition monitoring, image processing, speech, and biomedicine. This work involves the development of novel DSP methods for

the analysis of nonlinear or time-varying systems, statistical modeling (using Bayesian techniques), and adaptive algorithms.



Timothy G. Leighton received the M.A. degree in natural sciences and the Ph.D. degree in physics from the Cavendish Laboratory, Cambridge University, Cambridge, U.K., in 1985 and 1988, respectively.

He is a Professor of Ultrasonics and Underwater Acoustics and the Director of Postgraduate Research at the Institute of Sound and Vibration Research at the University of Southampton, Southampton, U.K. His research interests are in acoustic oceanography, biomedical ultrasonics, sonochemistry, and physical acoustics.

Dr. Leighton is a Fellow of the Acoustical Society of America, the Institute of Physics, and the Institute of Acoustics.



Jonathan M. Bull received the B.Sc. degree in geology and geophysics from University of Durham, Durham, U.K., in 1987 and the Ph.D. degree in marine geophysics from University of Edinburgh, Edinburgh, U.K., in 1990.

He is currently a Professor of Geophysics at the National Oceanography Centre Southampton, University of Southampton, Southampton, U.K. His research interests include near-surface geophysics, active faulting, and the development of novel 3-D subsurface imaging technology.



Andy Harris has over 30 years experience in electroacoustic research and development. He is an Acoustics Researcher at the National Marine Facility, National Oceanography Centre Southampton, University of Southampton, Southampton, U.K. His research interests are in specialized transducers for geophysics, bioacoustics, and long-range communications.